Supplementary Information

Highly efficient organic solar cells based on simple polymer donor derived from difluorinated benzene-quarterthiophene skeleton

Zesheng Zhang[ab]‡, Lingchen Kong[a]‡, Chao Liu[bc], Hua Tang[bc], Xinkang Wang[a], Mingqing Chen[a], Mei Luo[a], Lianjie Zhang[a]*, Cheng Liu[d], Xuncheng Liu[d]*, Dongge Ma[a], Christoph J. Brabec[bc]*, Junwu Chen[a]*

[a]*Institute of Polymer Optoelectronic Materials and Devices, Guangdong Basic Research Center of Excellence for Energy and Information Polymer Materials, State Key Laboratory of Luminescent Materials and Devices, South China University of Technology, Guangzhou 510640, P. R. China.* ***E-mail:*** *lianjiezhang@scut.edu.cn; psjwchen@scut.edu.cn*

[b]*Institute of Materials for Electronics and Energy Technology (i-MEET), Friedrich-Alexander-Universität Erlangen-Nürnberg (FAU), 91058 Erlangen, Germany.* ***E-mail:*** *christoph.brabec@fau.de*

[c]*Helmholtz-Institute Erlangen-Nürnberg (HI ERN), Immerwahrstraße 2, 91058 Erlangen, Germany*

[d]*College of Materials and Metallurgy, Guizhou University, Guiyang 550025, P. R. China.* ***E-mail:*** *xcliu3@gzu.edu.cn*

‡ These authors are equally contributed.

1. Synthesis

Synthesis of compound 1 (5,5'-(2,3-difluoro-1,4-phenylene) bis(3-(2-octyldodecyl)thiophene)). To a solution of 1,4-dibromo-2,3-difluorobenzene (0.82 g, 3 mmol) and tributyl(4-(2-octyldodecyl)thiophen-2-yl)stannane (4.31 g, 6.6 mmol) in *o*-xylene (10 mL) was added $Pd(PPh_3)_4$ (173 mg, 0.15 mmol) under argon. The mixture was heated to 120 ºC and stirred overnight. After removal of the solvent, the crude product was purified via column chromatography (silica gel) by using petroleum ether as eluent to give compound 1 as a white solid (2.27 g, 90%). ^{1}H NMR (500 MHz, Chloroform-*d*) δ 7.38-7.28 (m, 4H), 6.95 (s, 2H), 2.57 (d, 4H), 1.64 (dd, 2H), 1.38-1.14 (m, 64H), 0.87 (t, 12H). ^{13}C NMR (125 MHz, Chloroform-*d*) δ 149.19, 146.83, 143.01, 135.37, 128.80, 122.50, 121.91, 77.03, 38.90, 35.03, 33.36, 33.34, 31.97, 30.04, 29.73, 29.71, 29.68, 29.41, 29.39, 26.65, 22.73, 14.15.

Synthesis of compound 2 5,5'-(2,5-difluoro-1,4-phenylene) bis(2-bromo-3-(2-octyldodecyl)thiophene). To a solution of compound 1 (1.68 g, 2 mmol) in THF (30 mL) was added N-Bromosuccinimide (NBS) (0.75 g, 4.2 mmol) at 0 ºC. The mixture was stirred overnight. After removal of the solvent, the crude product was purified via column chromatography (silica gel) by using petroleum ether as eluent to give compound 2 as a white solid (1.89 g, 95%). ^{1}H NMR (500 MHz, Tetrachloroethane-d_2) δ 7.34 (d, 2H), 7.23 (s, 2H), 2.58 (d, 4H), 1.80-1.71 (m, 2H), 1.32 (dd, 64H), 0.93 (t, 12H). ^{13}C NMR (125 MHz, Chloroform-*d*) δ 149.22, 146.70, 142.33, 134.93, 128.34,

122.07, 111.28, 77.03, 38.54, 34.27, 33.38, 33.37, 31.98, 31.96, 30.02, 29.73, 29.71, 29.70, 29.65, 29.41, 29.39, 26.56, 22.74, 22.73, 14.15.

Synthesis of Po2F. To a mixture of compound 2 (150 mg, 0.15 mmol), 5,5'-bis(trimethylstannyl)-2,2'-bithiophene (79 mg, 0.15 mmol), $Pd_2(dba)_3$ (4.5 mg, 0.005 mmol) and $P(o\text{-}Tol)_3$ (15.3 mg, 0.05 mmol) in a Schlenk flask was added *o*-xylene (5 mL) under argon. The mixture was heated to 130 ºC for 72 h. Then the solution was cooled to room temperature and added into 150 mL methanol dropwise. The precipitate was collected and further purified via Soxhlet extraction by using *n*-hexane, dichloromethane, chloroform and chlorobenzene in sequence. The chlorobenzene fraction was concentrated and added into methanol dropwise. The precipitate was collected and dried under vacuum overnight to give Po2F as a red solid (136 mg, 85%). The M_n for Po2F is 69.5.6 KDa, with a PDI of 1.25.

Synthesis of compound 3 5,5'-(2,5-difluoro-1,4-phenylene)bis(3-(2-octyldodecyl)thiophene). Compound 3 was synthesized utilizing the identical procedure employed for the synthesis of compound 1, yielding a pristine white solid as the final product. (2.28 g, 90%). ^{1}H NMR (500 MHz, Chloroform-*d*) δ 7.36 (t, 2H), 7.30 (s, 2H), 6.94 (s, 2H), 2.56 (d, 4H), 1.62 (td, 2H), 1.36-1.17 (m, 64H), 0.87 (t, 12H). ^{13}C NMR (125 MHz, Chloroform-*d*) δ 156.08, 153.62, 142.96, 135.25, 128.74, 122.09, 115.12, 77.35, 77.03, 76.71, 38.89, 35.03, 33.34, 33.32, 31.95, 30.03, 29.72, 29.69, 29.66, 29.39, 29.37, 26.64, 22.72, 14.14.

Synthesis of compound 4 5,5'-(2,5-difluoro-1,4-phenylene)bis(2-bromo-3-(2-octyldodecyl)thiophene). Compound 4 was synthesized utilizing the identical procedure employed for the synthesis of compound 2, yielding a pristine white solid as the final product. (1.88 g, 95%). ^{1}H NMR (500 MHz, Tetrachloroethane-d_2) δ 7.29 (t, 2H), 7.14 (s, 2H), 2.50 (d, 4H), 1.67 (t, 2H), 1.40-1.11 (m, 64H), 0.86 (t, 12H). ^{13}C NMR (125 MHz, Chloroform-*d*) δ 156.04, 153.58, 142.22, 134.76, 128.12, 121.43, 114.38, 77.35, 77.03, 76.71, 38.55, 34.26, 33.38, 33.36, 31.97, 31.96, 30.02, 29.73, 29.70, 29.65, 29.41, 29.39, 26.56, 22.74, 22.73, 14.15.

Synthesis of Pp2F. Pp2F was synthesized utilizing the identical procedure employed for the synthesis and purification of Po2F, yielding a red solid as the final product. (131 mg, 82%). The M_n for Pp2F is 59.5 KDa, with a PDI of 2.07.

Synthetic complexity (SC) analysis:

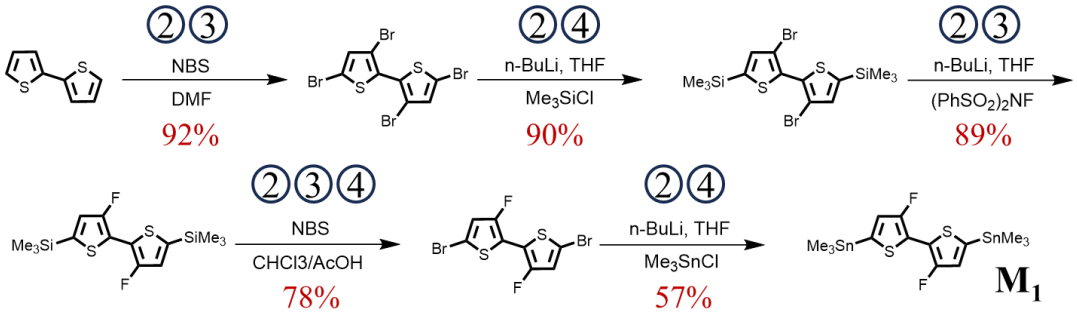

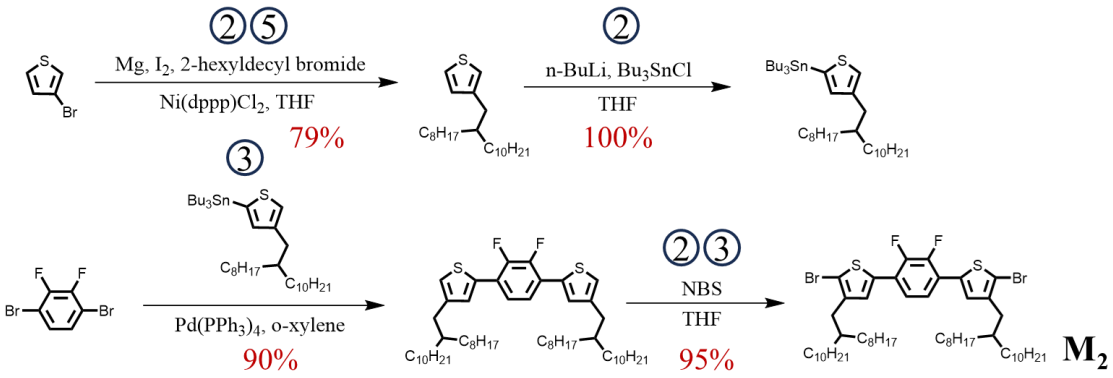

Fig. S1. Synthetic routes of the monomers M_1 and M_2 (The unit operations are represented by codes: 1 = Quenching/neutralization, 2 = Extraction, 3 = Column chromatography, 4 = Recrystallization, 5 = Distillation/sublimation).

Synthetic complexity (SC) analysis[1, 2]: The assessment of synthetic complexity (SC) involves the consideration of five parameters:

1) Number of Synthetic Steps (NSS)
2) Reciprocal Yields of the Monomers (RY)
3) Number of Unit Operations Required for the Isolation/Purification of the Monomers (NUO)
4) Number of Column Chromatographic Purifications Required by the Monomers (NCC)
5) Number of Hazardous Chemicals Used for Their Preparation (NHC)

The synthetic complexity (SC) can then be calculated using the following equation:

$$SC = 35\frac{NSS}{NSS_{max}} + 25\frac{RY}{RY_{max}} + 15\frac{NUO}{NUO_{max}} + 15\frac{NCC}{NCC_{max}}$$

Each parameter is assigned an empiric coefficient, representing its relative importance in the assessment. The weights assigned to NSS, RY, NUO, NCC, and NHC are 35, 25,

15, 15, and 10, respectively.

To enhance the precision in evaluating cost-effectiveness, an average synthetic complexity (ASC) is proposed for assessing commercial potential. It is calculated as follows:

$$ASC = SC_D w_D + SC_A w_A$$

where w denotes the weight ratio in the blend, with subscripts D and A indicating donor and acceptor materials, respectively.

Figure-of-merit (FOM) analysis involves assessing the average total cost of the polymer donors in terms of the SC as input and the PCE as output:

$$FOM = \frac{SC}{PCE}$$

Average FOM (AFOM) is proposed to evaluate cost-effectiveness of donor:acceptor combination in OSCs.

$$AFOM = \frac{ASC}{PCE}$$

2. Measurements and characterization

Nuclear magnetic resonance (NMR): ^{1}H and ^{13}C NMR spectra were acquired employing a Bruker AV-500 MHz spectrometer in deuterated solvents at room temperature. Chemical shifts were referenced to tetramethylsilane (TMS) as the internal standard.

Gel permeation chromatography (GPC): The molecular weights of Po2F and Pp2F were determined utilizing a PL-GPC 220 high-temperature chromatography system in 1,2,4-trichlorobenzene (TCB) at 150°C. A calibration curve of polystyrene standards was employed for accurate measurement.

Thermogravimetric analysis (TGA): TGA measurements were performed using a METTLER TOLEDO (TGA 2 STAR system) apparatus, employing a heating rate of 20 °C min^{-1} under a nitrogen atmosphere.

Differential scanning calorimetry (DSC): DSC measurements were performed on a TA (DSC2500) apparatus under a nitrogen atmosphere with a heating/cooling rate of 10/10 °C min^{-1} for the first and second cycle.

UV-vis absorption spectra: UV-vis absorption spectra of the polymers in chlorobenzene solution and films were measured using a SHIMADZU UV-3600 spectrophotometer.

Cyclic voltammetry (CV): Cyclic voltammetry measurements were conducted utilizing a CHI630E electrochemical workstation equipped with a three-electrode configuration. The reference electrode employed was Ag/AgCl, the counter electrode was a platinum plate, and the working electrode was glassy carbon. The supporting electrolyte used was tetrabutylammonium hexafluorophosphate in anhydrous

acetonitrile (0.1 mol L^{-1}). An internal standard, the ferrocene/ferrocenium (Fc/Fc^{+}) redox couple, with an assigned absolute energy of –4.8 eV versus vacuum, was utilized. The HOMO energy levels of the samples were determined using the equation $E_{HOMO} = -e\ (E_{ox\ onset} + 4.8 - E_{1/2}^{(Fc/\ Fc+)})$, where *E*ox onset represents the onset of oxidation potential relative to the measured Fc/Fc^{+} redox couple. The LUMO energy levels were determined using the equation $E_{LUMO} = E_{HOMO} + E_g^{opt}$, where E_g^{opt} represents the optical bandgap of the polymer as a thin film. The Fc/ Fc^{+} redox couple was observed at 0.45 V relative to the Ag/Ag^{+} electrode.

Density functional theory (DFT) calculation: DFT calculations were conducted by employing the Gaussian 16 package at the B3LYP/6-31G(d,p) level to simulate the molecular geometry of the polymers. In these simulations, the polymer skeleton was represented by two repeat units, and all alkyl side chains were substituted with methyl groups to simplify the computational complexity.

Atomic force microscopy (AFM): AFM images were captured using a Bruker Multimode 8 Microscope AFM operated in tapping-mode.

Transmission electron microscope (TEM): TEM images were obtained conducting a JEM-2100F transmission electron microscope operated at 200 kV.

Grazing incidence wide-angle X-ray scattering (GIWAXS): 2D-GIWAXS was

conducted employing a Xeuss 2.0 small angle X-ray scattering instrument from Xenocs, France. The instrument features a Pilatus 3R 1M detector from Dectris, boasting an effective detection area of 168.7×179.4 mm^2, a pixel size of 0.172×0.172 mm^2, a 2D image resolution of 981×1043 pixel, and a dynamic range of 20 bits. The X-ray source utilized is a MetalJet D2 liquid metal target light source with maximum power 300W, and the wavelength employed is λ = 1.34144 Å. The detector traverses within a vacuum chamber with a sample-to-detector distance of 214.545 mm. The combination of minimized background scattering and a high-performance detector facilitates detectable q-range spanning from 0.1 to 2.0 $Å^{-1}$. The sample was positioned vertically on the goniometer and tilted to a glancing angle of 0.2° relative to the incident beam. A small beam was employed to enhance resolution. The accumulation time was 1 hours for each measurement. In-plane and out-of-plane line-cuts were obtained using Fit 2D program.

Contact angle: The surface energy of films was obtained by VCA15 surface contact angle analyzer (Data physics). The droplets of water and ethylene glycol (EG) were dripped on the neat films. The surface tension (γ) is estimated by the Wu method[3].

3. Device fabrication and characterization

Fabrication of field-effect transistor (OFET): OFET devices, based on Po2F and Pp2F, were fabricated employing a conventional bottom gate, top contact architecture. These transistors featured highly doped Si as the gated electrode, while gold (Au) served dual roles as both the source and drain electrodes. Substrate preparation involved

a rigorous cleaning regimen, comprising successive sonication steps with soap water, deionized water, acetone, and absolute ethanol. Subsequently, the gate dielectric layers on the substrates underwent modification via *n*-octadecyltrichlorosilane (OTS) treatment, achieved through submersion in a solution of OTS in toluene. Both Po2F and Pp2F films were prepared from solutions (chlorobenzene as solvent, 8.0 mg/mL) via spin-coating at 2500 rpm for 35 seconds onto the OTS-treated substrates. Notably, the films underwent thermal annealing at 200 °C for 10 minutes on a hotplate within a nitrogen glovebox. Gold contacts, measuring 40 nm in thickness, were precisely evaporated onto the polymer film layer through a meticulously positioned metal mask to define channels of 80 μm in length and 1400 μm in width. The film thickness of the resultant devices ranged from 60 to 100 nm. Field-effect mobility was calculated utilizing the standard equation applicable to the saturation region in metal-oxide-semiconductor field-effect transistors, delineated as follows:

$$Ids = \mu \frac{W}{2L} C_i (V_G - V_T)^2$$

where, *Ids* represents the drain-source current, μ denotes the field-effect mobility, W and L denote the channel width and length, respectively, C_i signifies the capacitance per unit area of the gate insulator (C_i = 10 nF cm^{-2}), while V_G and V_T represent the gate voltage and threshold voltage, respectively.

Fabrication of organic solar cells (OSCs): The patterned indium tin oxide (ITO) glass substrates were meticulously cleaned through a series of steps: first, they underwent sonic cleaning in a detergent solution, followed by rinsing with deionized water,

acetone, and isopropanol, both at room temperature and in an ultrasonic water bath, each step lasting 10 minutes. Subsequently, the substrates received oxygen plasma treatment at room temperature for 10 minutes. Once cleaned and treated, a layer of PEDOT:PSS was uniformly spin-coated onto the ITO glass substrates at 4000 rpm for 30 s, followed by baking at 150 °C for 10 minutes to ensure adhesion and stability. Afterward, the substrates were transferred to a nitrogen-filled glove box to maintain an inert atmosphere. A solution of the polymer donor was prepared in chlorobenzene and spin-coated onto the substrates at various rates to achieve films of different thicknesses. Subsequently, a solution of Y6BO in chloroform was spin-coated onto the polymer donor film. The resulting films underwent annealing at 80 °C for 5 minutes. To enhance the film properties further, solvent annealing was performed by placing the films in a petri dish containing carbon disulfide for 5 minutes. Following this, a layer of PDINN (10 nm) was spin-coated from a methanol solution (1.5 mg mL^{-1}) at a speed of 3000 rpm for 30 s. Finally, a 100 nm thick layer of silver was deposited via thermal evaporation through a shadow mask in a vacuum chamber with a pressure of 4×10^{-6} Pa, completing the fabrication process. The devices, with an active area of 0.07 cm^2, were characterized using a 0.04 cm^2 aperture mask to ensure accurate measurements.

Characterization of solar cells: The current density-voltage (*J-V*) characteristics were captured utilizing a Keithley 2400 source meter. Prior to testing, the light intensity of the illumination source underwent meticulous calibration via a standard silicon solar cell in conjunction with a KG5 filter, as validated by a National Renewable Energy

Laboratory (NREL) certified silicon photodiode. This meticulous calibration procedure yielded a calibrated light intensity value of 100 mW cm^{-2}, establishing a reliable baseline for subsequent experimental analyses.

External quantum efficiencies (EQEs): The EQE spectra were performed using a commercial EQE measurement system (Taiwan, Enlitech, QE-R3011). The light intensity each wavelength was calibrated by a standard single-crystal Si photovoltaic cell.

Transient photocurrent (TPC) and transient photovoltage (TPV): The TPC and TPV measurements of devices were meticulously assessed through the application of 500 nm laser pulses characterized by a pulse width of 120 fs and low pulse energy, specifically on the short-circuit devices in a light-deprived environment. The laser pulses were generated via an advanced optical parametric amplifier (TOPAS-Prime), which was pumped by a mode-locked Ti: sapphire oscillator seeded regenerative amplifier. This amplifier boasted a remarkable pulse energy of 1.3 mJ at 800 nm, coupled with an impressive repetition rate of 1 Hz (spectra Physics Spitfire Ace).

Fabrication and characterization of single-carrier devices: Hole-only and electron-only devices were fabricated to measure the hole and electron mobilities of the active layers, employing the space charge limited current (SCLC) method. The configuration for hole-only devices comprised ITO/PEDOT:PSS/active layer/MoO_3/Ag, while

electron-only devices were structured as ITO/ZnO/active layer/PDINN/Ag. To determine the mobilities (μ_h or μ_e), the dark current was meticulously fitted to the model of a single carrier SCLC, characterized by the equation:

$$J = \frac{9}{8}\varepsilon_0\varepsilon_r\mu\frac{V^2}{d^3}$$

Here, J represents the current, ε_0 is the permittivity of free space, ε_r denotes the relative permittivity of the material, d signifies the thickness of the active layers and V represents the effective voltage. The effective voltage is derived by subtracting the built-in voltage (V_{bi}) from the applied voltage (V_{appl}), $V=V_{appl} - V_{bi}$. Consequently, the mobility can be calculated from the slope of the $J^{1/2}$-V curves.

Film-depth-dependent Light Absorption Spectroscopy (FLAS)[4-7]: The FLAS were acquired using a light absorption spectrometer (PU100, Puguangweishi Co. Ltd). To obtain depth-resolved data for the organic active layer, in-situ oxygen plasma etching was performed at low pressure (< 25 Pa). Exciton generation profiles were simulated based on a modified optical transfer matrix method, incorporating depth-resolved absorption spectra and optical interference effects. Detailed information on the FLAS characterization can be found in the literature.

Transient Absorption Spectroscopy (TAS): The TAS measurements were conducted utilizing a Femtosecond Transient Absorption (TA) spectrometer, specifically the Ultrafast System HARPIA TA spectrometer. This setup includes a laser generator by KGW amplifier (PHAROS, Light Conversion), an optical parametric amplifier

(ORPHEUS twins, S/N:P19340, Light Conversion), and an ultrafast spectroscopic stem (HARPIA-TA, M19032, Light Conversion). The laser beam center is 1030 nm, with a pulse duration of approximately 100 fs and a repetition rate of 25 kHz. For probing, a white light continuum probe beam was generated employing a nonlinear medium made of sapphire crystal. The transmitted probe beam passing through the sample was recorded using a CCD linear Si detector coupled to a monochromator. This setup allowed for the investigation of ultrafast dynamics in the sample by observing changes in absorption over very short time scales.

Time-resolved photoluminescence (TRPL): TRPL spectrum were measured employing the Horiba Fluorolog-3 Time-Correlated Single Photon Counting system. For the polymer donors, TRPL curves were stimulated by a 500 nm laser, while for Y6BO, a 750 nm laser was employed.

FTPS-EQE measurements: FTPS-EQE was recorded on a FTPS (PECT-600) system (Enlitech), where a low-noise current amplifier was employed to amplify the photocurrent generated from the photovoltaic devices with illumination light modulated by the Fourier transform infrared (FTIR) instrument.

Electroluminescence (EL) measurements: Current density (J)-luminance (L)-voltage (V) characteristics and EL spectra were recorded by a Photo Research PR745 and a commercial system (XPQY-EQE-350-1100)

4. Additional figures.

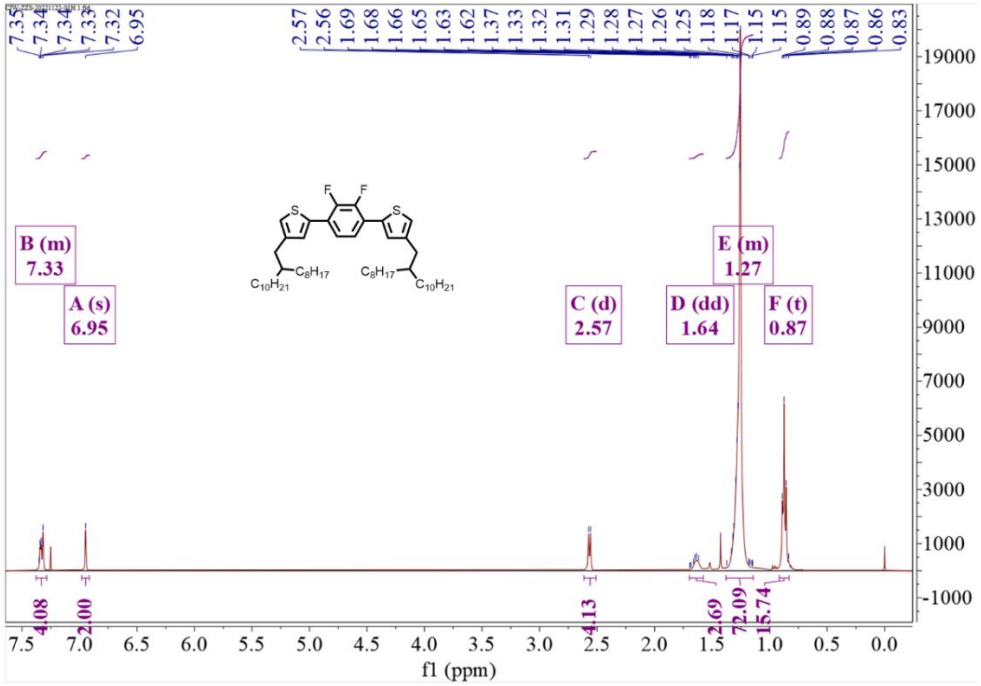

Fig. S2. ^{1}H NMR spectrum of the compound 1.

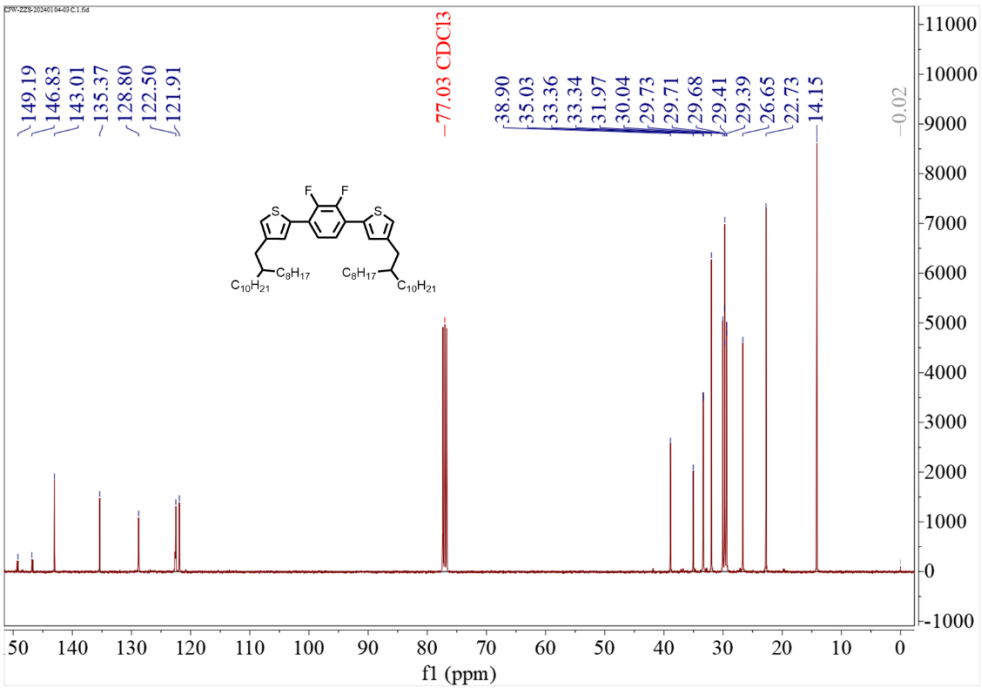

Fig. S3. ^{13}C NMR spectrum of the compound 1.

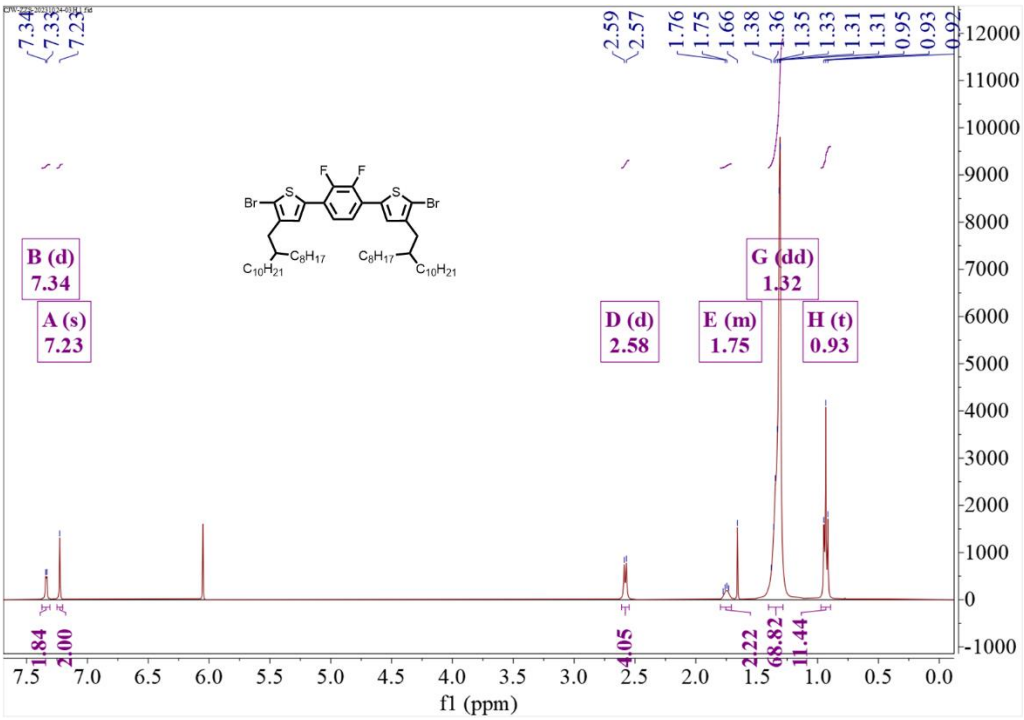

Fig. S4. ^{1}H NMR spectrum of the compound 2.

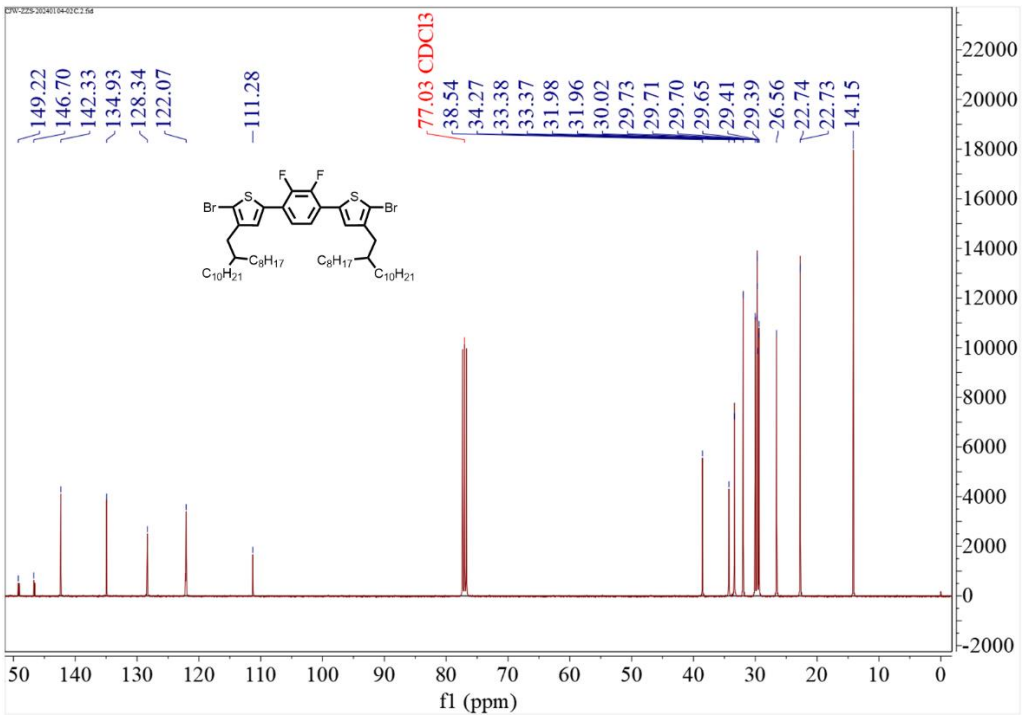

Fig. S5. ^{13}C NMR spectrum of the compound 2.

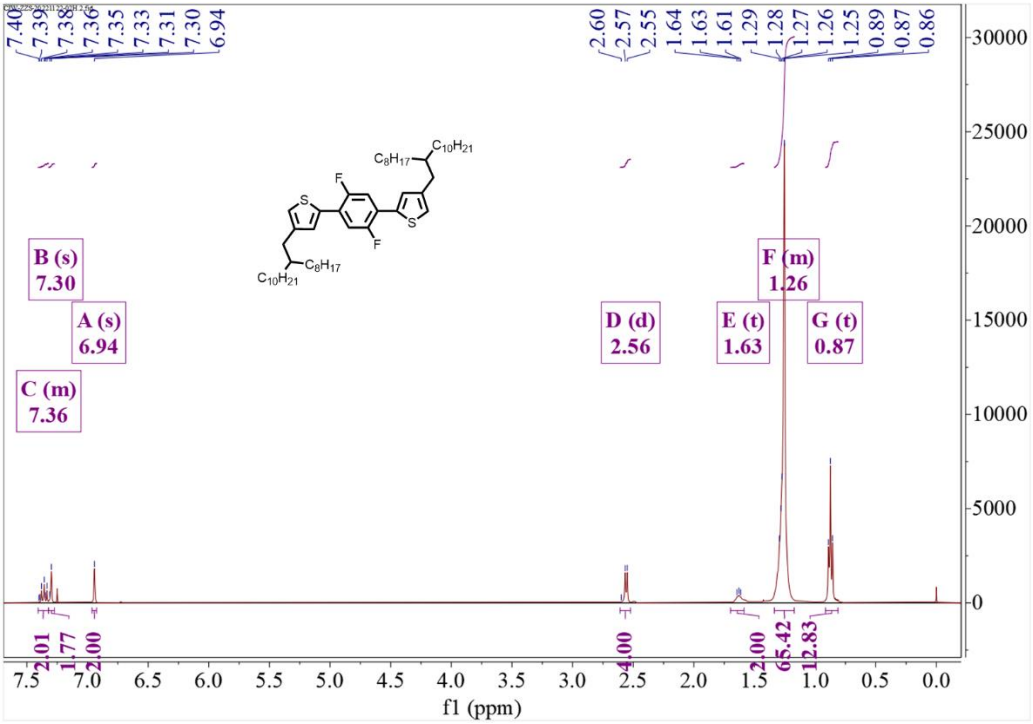

Fig. S6. ^{1}H NMR spectrum of the compound 3.

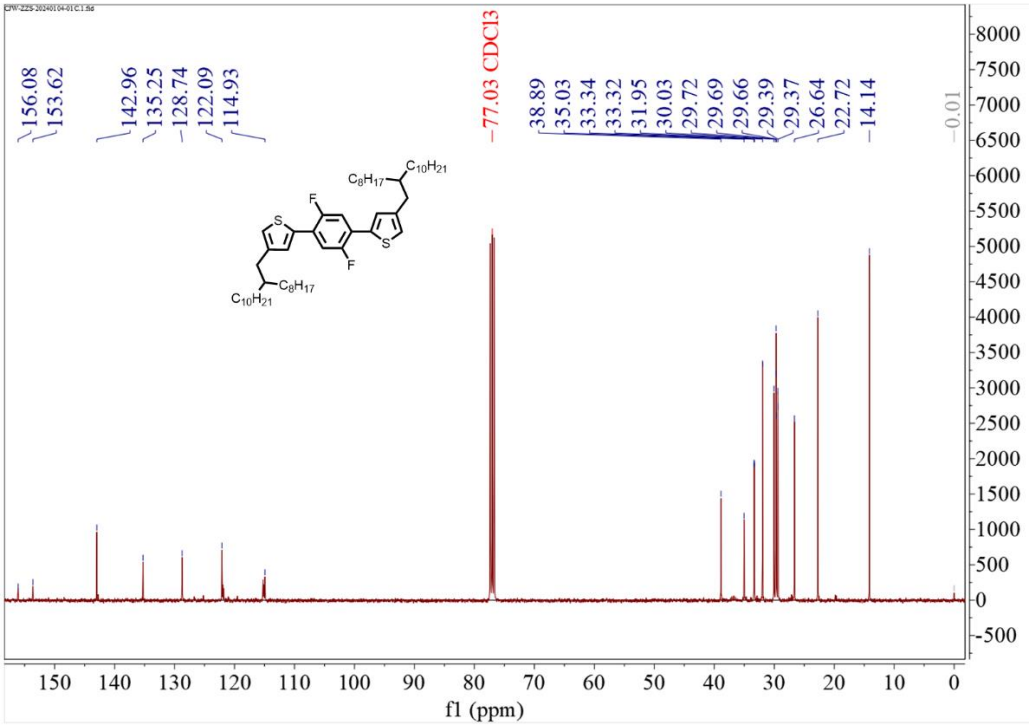

Fig. S7. ^{13}C NMR spectrum of the compound 3.

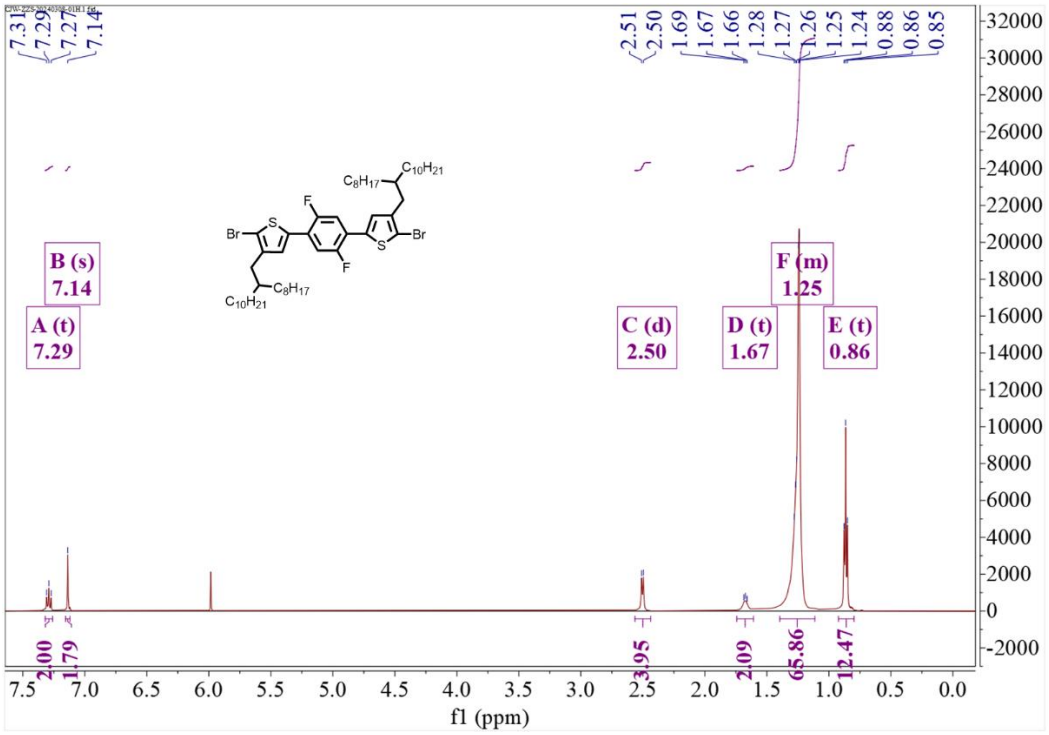

Fig. S8. ^{1}H NMR spectrum of the compound 4.

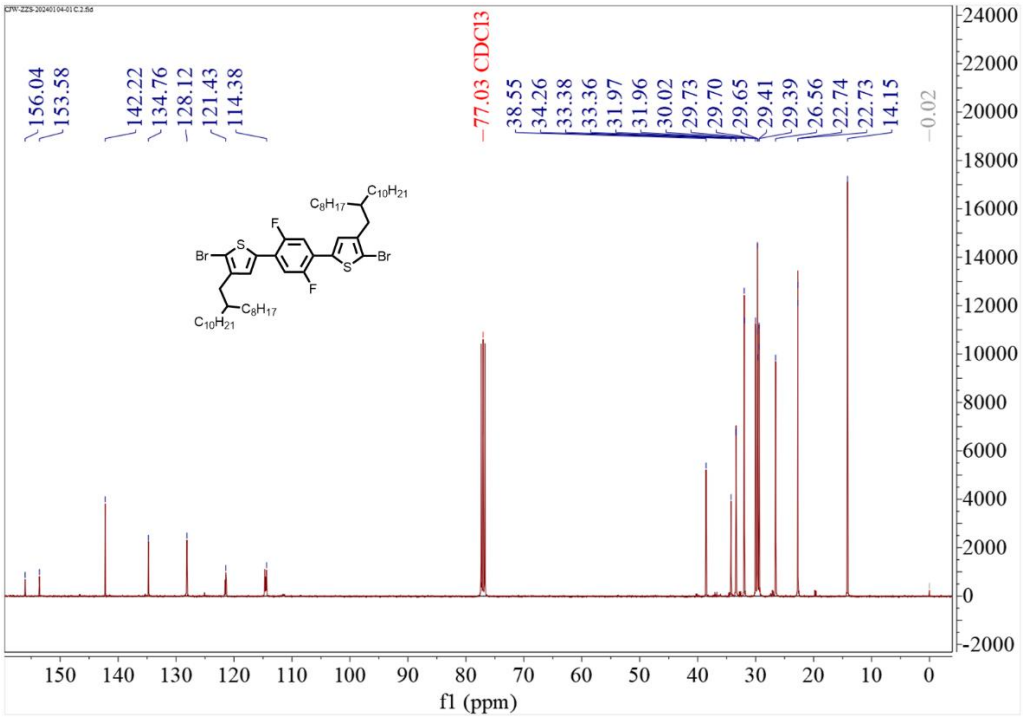

Fig. S9. ^{13}C NMR spectrum of the compound 4.

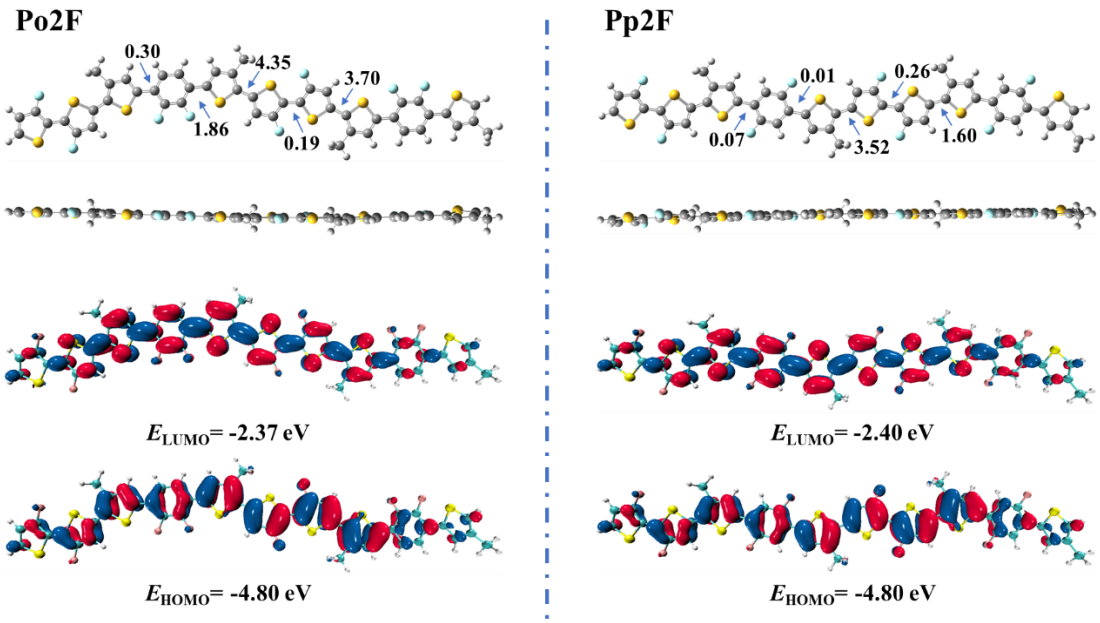

Fig. S10. Calculated molecular geometries and frontier molecular orbitals of Po2F and Pp2F dimers at B3LYP/6-31G(d) level.

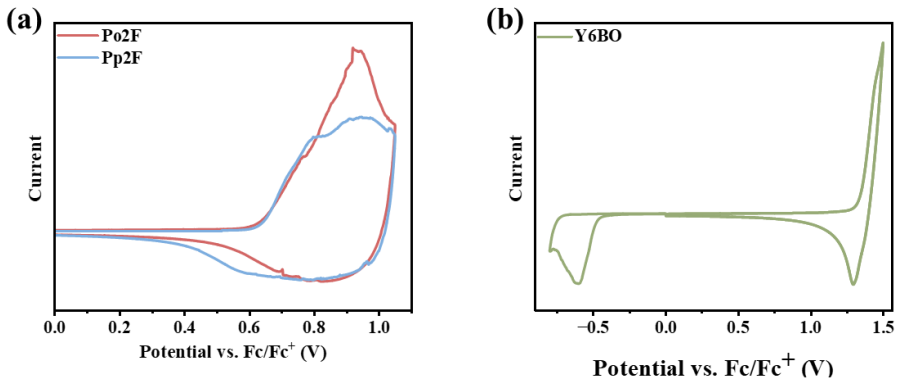

Fig. S11. Cyclic voltammograms of (a) Po2F, Pp2F and (b) Y6BO measured in acetonitrile.

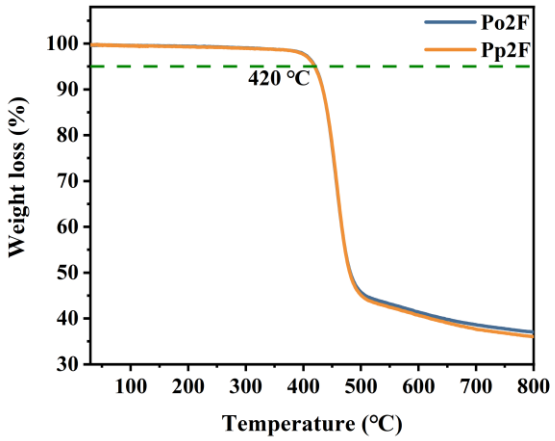

Fig. S12. TGA curves of Po2F and Pp2F.

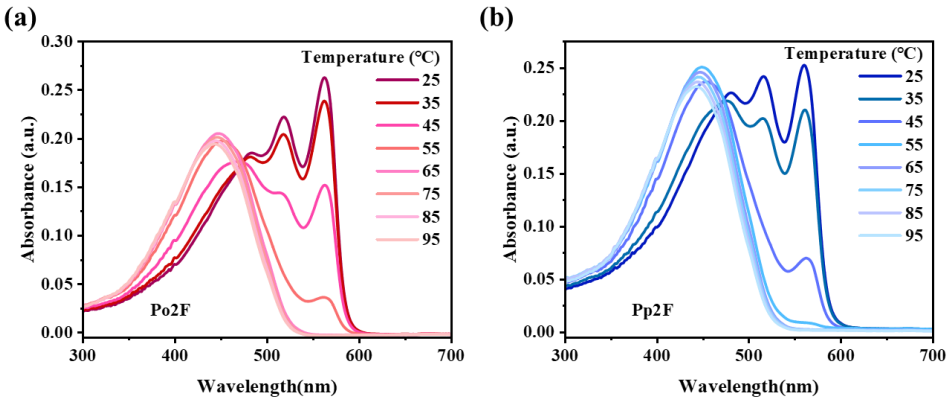

Fig. S13. The UV–vis absorption spectra of (a) Po2F and (b) Pp2F under different temperatures in chlorobenzene solutions.

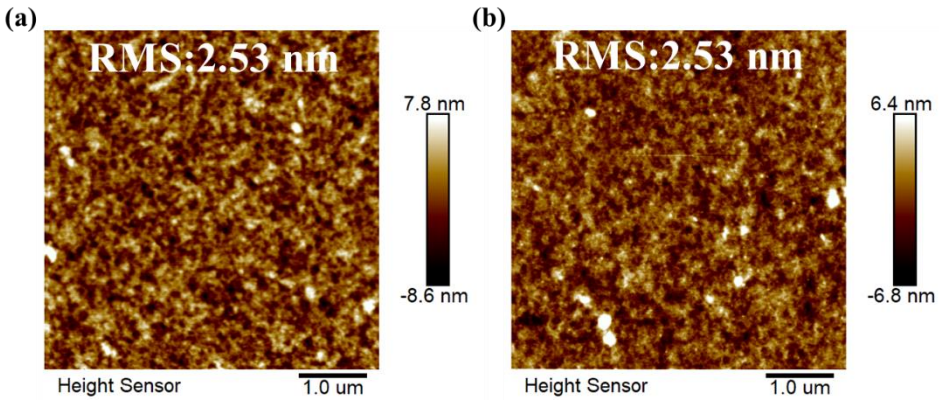

Fig. S14. AFM height images of Po2F (a) and Pp2F (b) neat films.

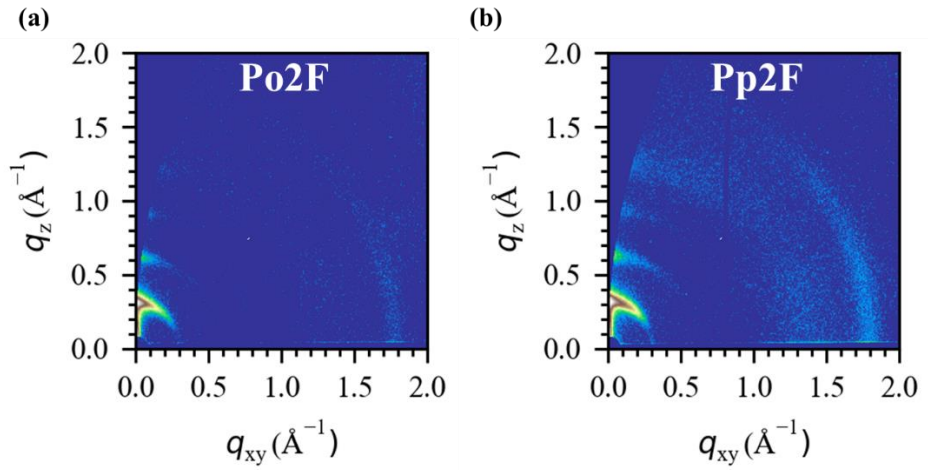

Fig. S15. 2D-GIWAXS pattern of Po2F (a) and Pp2F (b) neat films.

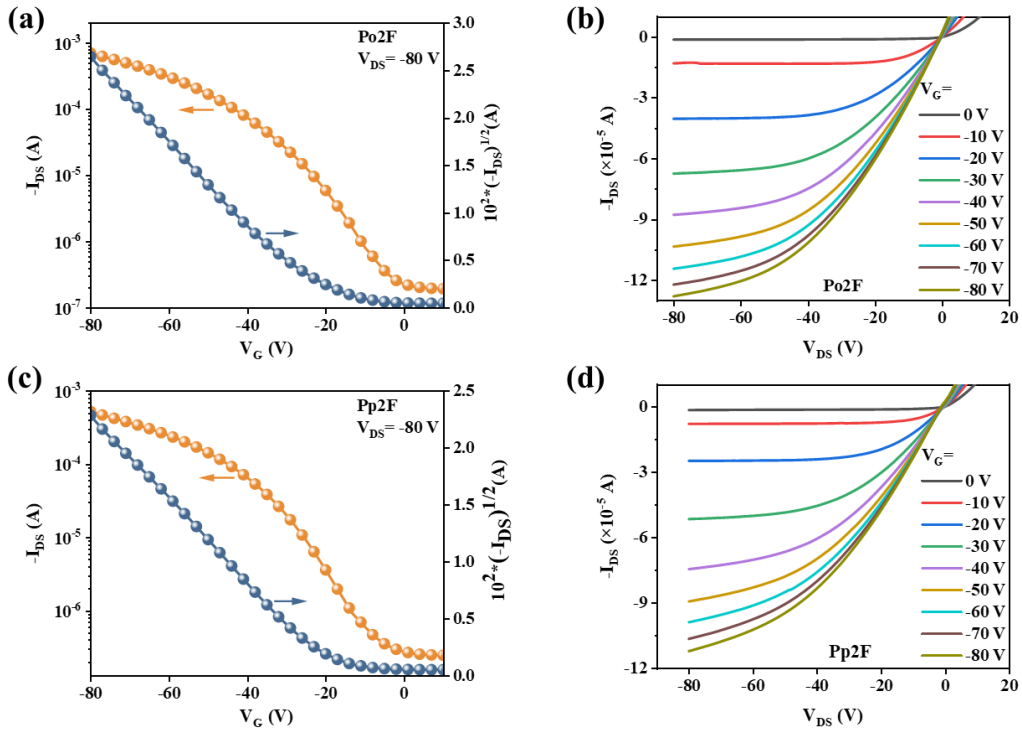

Fig. S16. OFET output (a, c) and transfer characteristics (b, d) of Po2F and Pp2F.

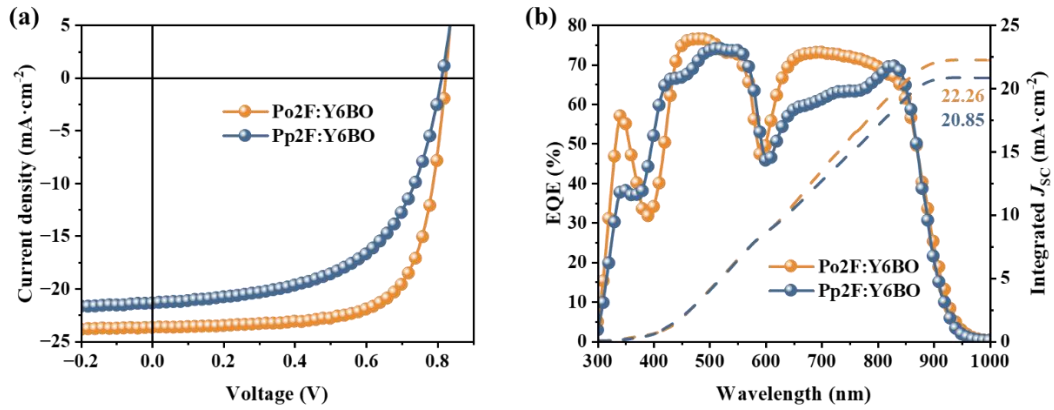

Fig. S17. (a) *J-V* characteristics, (b) EQE spectra of the bulk heterojunction (BHJ) OSCs based on Po2F: Y6BO and Pp2F:Y6BO.

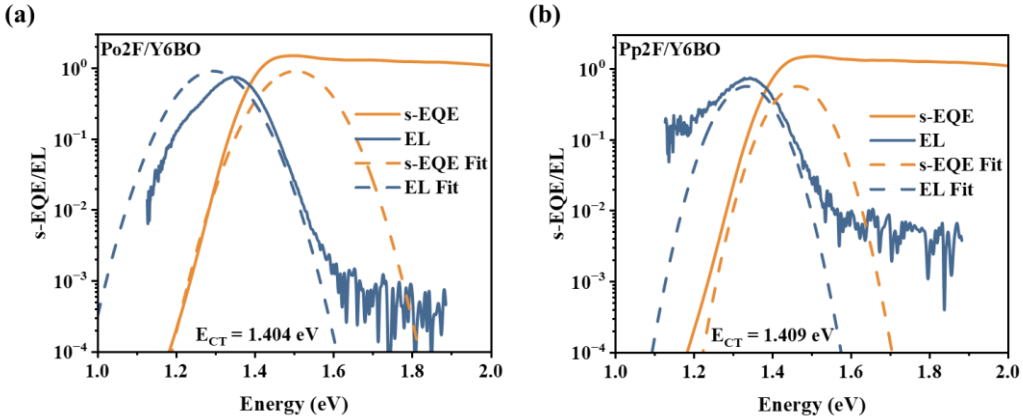

Fig. S18. s-EQE spectra and EQE_{EL} spectra of the OSCs based on Po2F/Y6BO (a) and Pp2F/Y6BO (b).

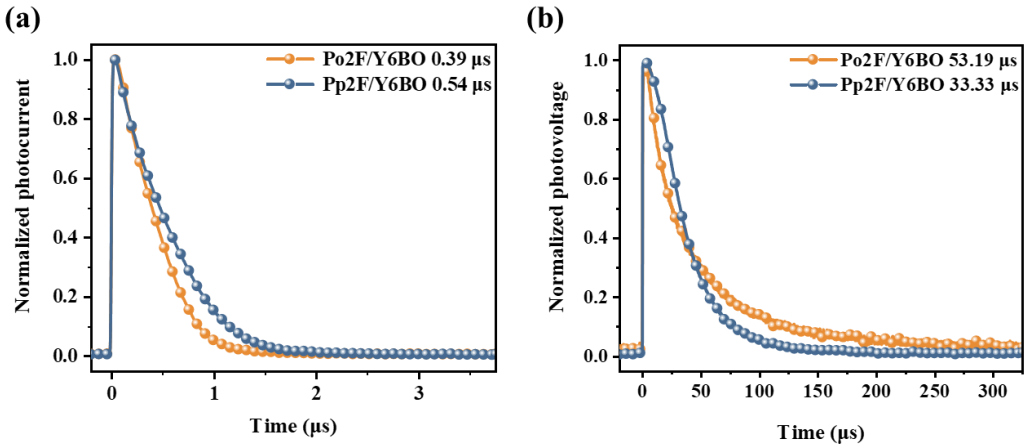

Fig. S19. TPC (a) and TPV (b) of the corresponding OSCs.

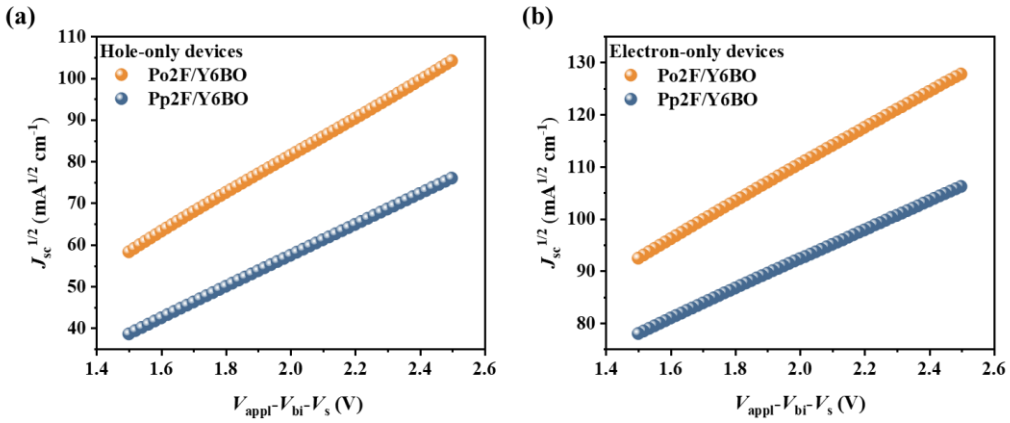

Fig. S20. The hole (a) and electron (b) mobilities based on Po2F/Y6BO and Pp2F/Y6BO LBL blend films which acquired from single-carrier devices.

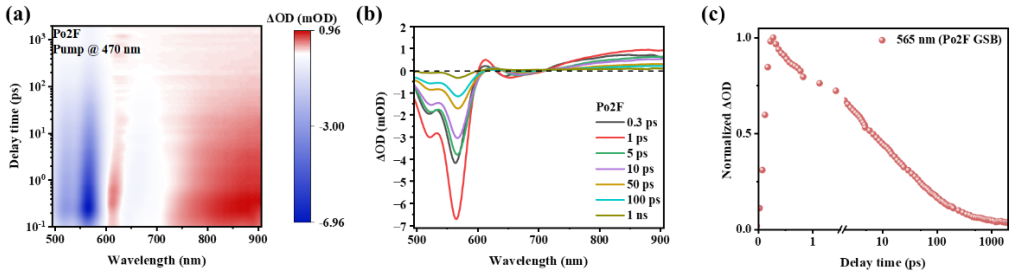

Fig. S21. 2D color plot of TAS (a), TAS spectra at different time delays (b), and kinetic traces probing at GSB (c) of Po2F.

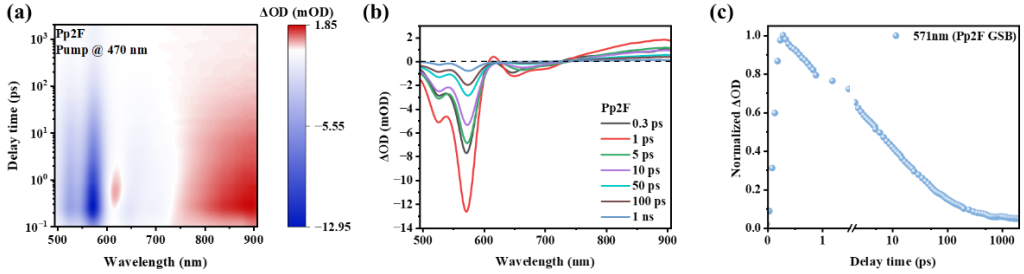

Fig. S22. 2D color plot of TAS (a), TAS spectra at different time delays (b), and kinetic traces probing at GSB (c) of Pp2F.

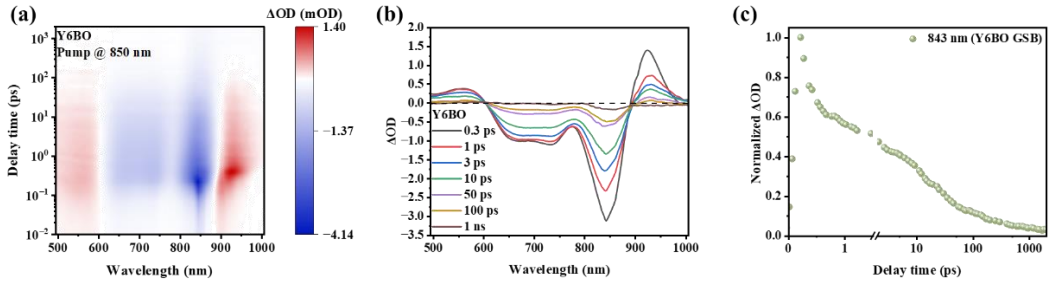

Fig. S23. 2D color plot of TAS (a), TAS spectra at different time delays (b), and kinetic traces probing at GSB (c) of Y6BO.

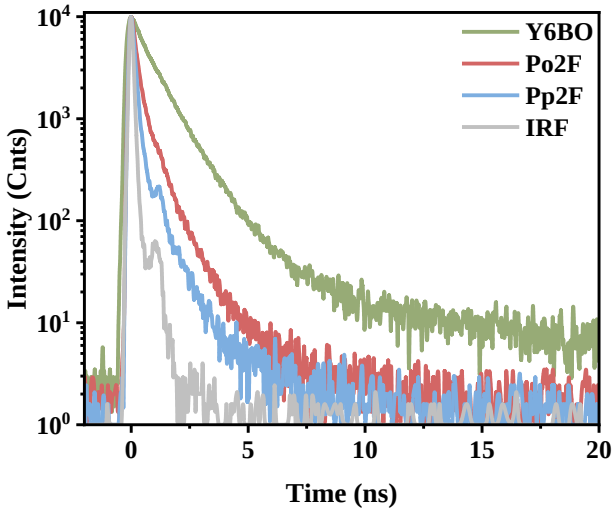

Fig. S24. TRPL spectra of Y6BO, Po2F, and Pp2F neat films.

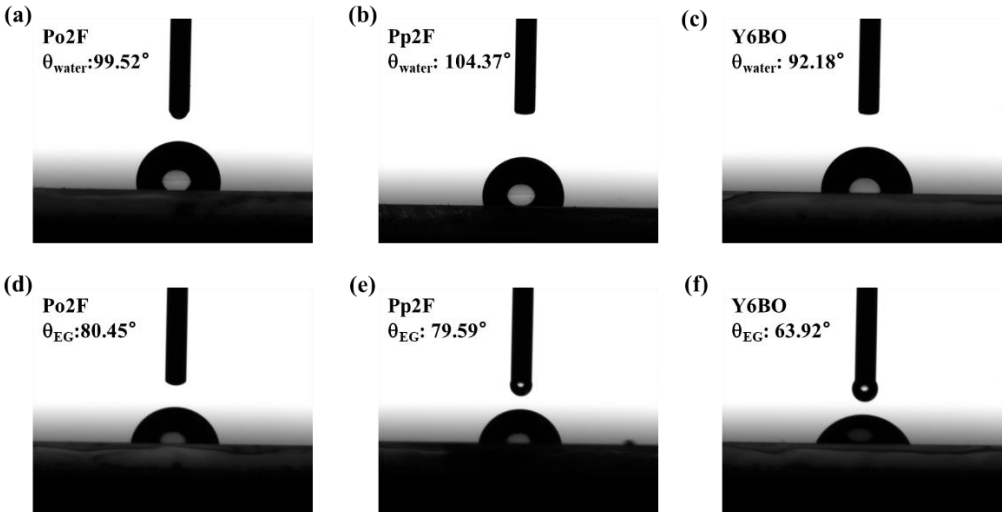

Fig. S25. Water (a-c) and ethylene glycol (d-f) contact angels on Po2F, Pp2F, and Y6BO films.

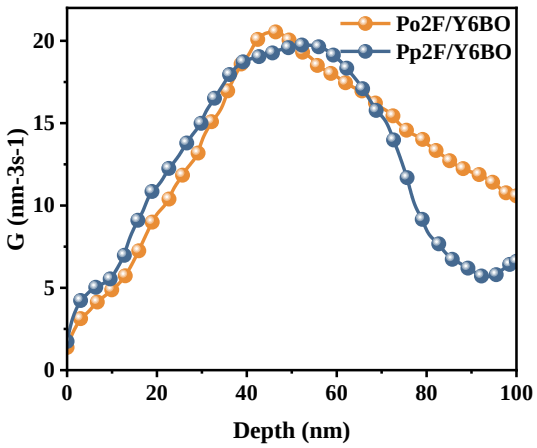

Fig. S26. Integration of exciton-production rate with respect to depth for Po2F/Y6BO and Pp2F/Y6BO LBL blend films.

5. Additional tables.

Table S1. GIWAXS parameters of Po2F, Pp2F, and Y6BO neat films.

Film	Out of plane (100)				In plane (010)			
	q_z (Å^{-1})	d spacing (Å)	FWHM[a] (Å^{-1})	CCL[b] (Å)	q_{xy} (Å^{-1})	π-π stacking (Å)	FWHM[a] (Å^{-1})	CCL[b] (Å)
Po2F	0.31	20.26	0.155	37.68	1.83	3.43	0.200	29.20
Pp2F	0.31	20.26	0.163	35.83	1.80	3.49	0.147	39.73

[a] FWHM is the full wide at the half maximum; [b] CCL=2πK/FWHM (K=0.93).

Table S2. OFET performance parameters of Po2F and Pp2F, fabricated under the optimal conditions.

Polymer	TA (°C)	μ_h[a] (cm^{2}V^{-1}S^{-1})	V_T (V)	I_{on}/I_{off}
Po2F	200	2.18 (1.96)	-17	10^3-10^4
Pp2F	200	1.54 (1.35)	-16	10^3-10^4

[a] Maximum mobilities with average values from at least five devices shown in parentheses.

Table S3. Photovoltaic parameters of the optimal BHJ OSCs based on Po2F: Y6BO and Pp2F:Y6BO under AM1.5G irradiation (100 mW cm^{-2}).

BHJ film	V_{OC} (V)	J_{SC} (mA cm^{-2})	$J_{sc\ cal}$ (mA cm^{-2})	FF (%)	PCE (%)
Po2F:Y6BO	0.832 (0.833 ± 0.002)	22.46 (22.67 ± 0.44)	22.26	69.19 (65.53 ± 2.01)	12.98 (12.42 ± 0.31)
Pp2F:Y6BO	0.814 (0.814 ± 0.004)	21.41 (20.14 ± 0.61)	20.85	57.22 (58.67 ± 0.65)	10.04 (9.62 ± 0.20)

Table S4. Photovoltaic parameters of the Po2F/Y6BO and Pp2F/Y6BO LBL-devices based on various polymer thickness under AM1.5G irradiation (100 mW cm^{-2}). (Upper layer Y6BO was kept at 50 nm).

LBL film	polymer thickness	V_{OC} (V)	J_{SC} (mA cm^{-2})	FF (%)	PCE (%)
Po2F/Y6BO	40	0.864	21.44	66.34	12.39
Po2F/Y6BO	50	0.861	22.08	67.54	12.93
Po2F/Y6BO	60	0.854	22.75	62.35	12.20
Pp2F/Y6BO	40	0.831	18.53	56.45	8.76
Pp2F/Y6BO	50	0.831	19.95	55.32	9.25
Pp2F/Y6BO	60	0.830	19.62	53.26	8.75

Table S5. Photovoltaic parameters of the Po2F/Y6BO and Pp2F/Y6BO LBL-devices based on various thermal annealing temperature under AM1.5G irradiation (100 mW cm^{-2}).

LBL film	TA (°C)	V_{OC} (V)	J_{SC} (mA cm^{-2})	FF (%)	PCE (%)
Po2F/Y6BO	70	0.840	22.84	66.86	12.70
Po2F/Y6BO	80	0.835	23.04	70.23	13.59
Po2F/Y6BO	90	0.825	23.20	68.87	13.10
Pp2F/Y6BO	70	0.818	19.82	59.08	9.60
Pp2F/Y6BO	80	0.814	21.41	57.22	10.04
Pp2F/Y6BO	90	0.810	20.44	58.77	9.61

Table S6. Photovoltaic parameters of the Po2F/Y6BO and Pp2F/Y6BO LBL-devices with or without solvent (carbon disulfide, CS_2) annealing under AM1.5G irradiation (100 mW cm^{-2}).

LBL film	SVA	V_{OC} (V)	J_{SC} (mA cm^{-2})	FF (%)	PCE (%)
Po2F/Y6BO	w/o	0.835	23.04	70.23	13.59
Po2F/Y6BO	w	0.850	24.23	74.81	15.45
Pp2F/Y6BO	w/o	0.814	21.41	57.22	10.04
Pp2F/Y6BO	w	0.827	21.91	66.74	12.14

Table S7. The summarized NSS, RY, NUO, NCC, NHC, and SC of monomers. The letters "A" and "N" represent the absolute value and the normalized value, respectively, where the values used for the normalization are NSS_{max} = 13, RY_{max} = 77, NUO_{max} = 25, NCC_{max} = 9, and NHC_{max} = 36[1, 2].

Monomer	Absolute values					*Normalized values*					*SC*
	NSS	RY	NUO	NCC	NHC	*NSS*	*RY*	*NUO*	*NCC*	*NHC*	
M_1	5	1.08	7	2	5	0.38	0.02	0.28	0.22	0.14	22.83
M_2	5	3.05	10	2	13	0.38	0.26	0.40	0.22	0.36	32.82

Table S8. The summarized NSS, RY, NUO, NCC, NHC, and SC of polymers. The letters "A" and "N" represent the absolute value and the normalized value, where the values used for the normalization are NSS_{max} = 22, RY_{max} = 86.9, NUO_{max} = 39, NCC_{max} = 13, and NHC_{max} = 44[1, 2].

Material	Absolute values					*Normalized values*					SC
	NSS	RY	NUO	NCC	NHC	*NSS*	*RY*	*NUO*	*NCC*	*NHC*	
Po2F	11	4.13	17	4	18	0.50	0.32	0.44	0.31	0.41	40.69
PDCBT	6	8.26	9	3	25	0.27	0.47	0.23	0.23	0.57	33.80
PDCBT-2F	10	8.51	18	5	33	0.45	0.48	0.46	0.38	0.75	47.85
PDCBT-Cl	8	8.07	14	4	32	0.36	0.47	0.36	0.30	0.73	41.55
P4T2FHD	9	5.45	17	5	25	0.41	0.38	0.43	0.38	0.57	41.70
P5TCN2F	11	5.31	19	5	28	0.50	0.37	0.49	0.38	0.64	46.15
P3HT	3	1.1	4	0	4	0.14	0.02	0.1	0	0.09	7.75
Y6	17	25.50	29	6	30	0.77	0.73	0.74	0.46	0.68	70.00
Y6BO	16	19.70	23	6	34	0.73	0.67	0.59	0.46	0.77	65.75
ZY4Cl	13	15.55	20	5	32	0.59	0.62	0.51	0.38	0.73	56.80
ITIC	11	7.70	23	6	19	0.50	0.46	0.59	0.46	0.43	49.05
ITIT-Th	11	18.46	16	6	30	0.50	0.65	0.41	0.46	0.68	53.60
IT-4F	12	8.24	21	7	21	0.55	0.47	0.54	0.54	0.48	52.00
O-IDTBR	17	6.67	28	7	28	0.77	0.43	0.72	0.54	0.64	63.00

[a)]The values of NSS, RY, NUO, NCC, NHC of these materials were cited from ref. 2, with the RY corrected according to corresponding literature.

Table S9. Parameters used for estimating the AFOM of OSCs based on reported polymer donors without fused-rings and polymer donors with fused-rings.

Combination	D:A ratio	SCD (%)	SCA (%)	ASC (%)	PCE (%)	AFOM (%)	Ref
Po2F:Y6BO	1:1	40.69	65.75	53.22	15.45	3.44	*This work*
P4T2F-HD: O-IDTBR	1:1.5	41.70	63.00	54.48	7.00	7.78	[8]
P3HT:O-IDTBR	1:1	7.80	63.00	35.40	6.30	5.62	[9]
PDCBT-2F:IT-4F	1:1	47.85	52.00	49.93	11.80	4.23	[10]
PDCBT:ITIC	1:1	33.80	49.05	41.43	10.16	4.08	[11]
P4T2F-HD:Y6-BO	1:1.2	41.70	65.75	54.82	13.65	4.01	[12]
PDCBT-Cl:ITIT-Th	1:1	41.55	53.60	47.58	12.38	3.84	[13]
P5TCN-2F:Y6	1:1	46.15	70	58.07	16.10	3.60	[14]
P5TCN-2F:Y6BO	1:1	46.15	65.75	55.95	15.80	3.54	[14]
P3HT:ZY-4Cl	1:1	7.80	56.8	32.3	10.24	3.15	[15]

[a)]The values of SCs of the donor and acceptor were cited from ref. 12.

Table S10. The SCLC hole mobility of Po2F/Y6BO and Pp2F/Y6BO LBL blend films acquired from single-carrier devices.

Blend	μ_h ($cm^2V^{-1}S^{-1}$)	μ_e ($cm^2V^{-1}S^{-1}$)	μ_h/μ_e
Po2F/Y6BO	1.19×10^{-3}	9.20×10^{-4}	1.29
Pp2F/Y6BO	8.05×10^{-4}	5.83×10^{-4}	1.38

Table S11. Fitted and calculated values of TAS for Po2F/Y6BO and Pp2F/Y6BO LBL blend films.

Blend	*Probe @*	A_1	τ_1 (ps)	A_2	τ_2 (ps)
Po2F/Y6BO	830 nm	0.44	2.19	0.46	43.55
Pp2F/Y6BO	830 nm	0.58	1.11	0.41	27.44
Po2F/Y6BO	552 nm	0.27	1.65	0.89	25.83
Pp2F/Y6BO	565 nm	0.50	2.38	0.91	30.88

Table S12. Fitted and calculated values of TRPL for Po2F, Pp2F, and Y6BO films.

Film	*Probe* @	A_1	τ_1 (ns)	A_2	τ_2 (ns)	τ (ns)
Y6BO	836 nm	0.054	7.320	6.128	1.000	1.380
Po2F	606 nm	0.105	1.900	1.515	0.534	0.802
Pp2F	606 nm	0.475	0.882	4.832	0.129	0.432

Table S13. GIWAXS parameters for edge-on orientation of Po2F/Y6BO and Pp2F/Y6BO films.

Film	Out of plane (100)				In plane (010)			
	q_z ($Å^{-1}$)	d spacing (Å)	FWHM[a] ($Å^{-1}$)	CCL[b] (Å)	q_{xy} ($Å^{-1}$)	π-π stacking (Å)	FWHM[a] ($Å^{-1}$)	CCL[b] (Å)
Po2F/Y6BO	0.32	19.63	0.175	33.37	1.75	3.59	0.401	14.56
Pp2F/Y6BO	0.32	19.63	0.106	55.10	1.75	3.59	0.229	25.50

Table S14. GIWAXS parameters for face-on orientation of Y6BO, Po2F/Y6BO, and Pp2F/Y6BO films.

Film	In plane (100)				Out of plane (010)			
	q_{xy} ($Å^{-1}$)	d spacing (Å)	FWHM[a] ($Å^{-1}$)	CCL[b] (Å)	q_z ($Å^{-1}$)	π-π stacking (Å)	FWHM[a] ($Å^{-1}$)	CCL[b] (Å)
Y6BO	0.40	15.70	0.186	31.40	1.76	3.57	0.422	13.84
Po2F/Y6BO	0.42	14.95	0.181	32.27	1.81	3.47	0.505	11.57
Pp2F/Y6BO	0.44	14.27	0.286	20.42	1.77	3.55	0.447	13.07

Table S15. Contact angle, surface free energy, and Flory–Huggins interaction parameters of Po2F, Pp2F, and Y6BO films.

Film	Contact angle (°)		Dispersion component γ^d (mN m^{-1})	Polar component γ^p (mN m^{-1})	Surface free energy γ (mN m^{-1})	χ donor:accptor
	θ_{water}	θ_{EG}				
Po2F	99.52	80.45	4.37	10.94	15.31	0.72K
Pp2F	104.37	79.59	2.19	12.94	15.13	0.76K
Y6BO	92.18	63.92	4.47	18.20	22.67	

Table S16. Photovoltaic parameters of the Po2F/PM6:L8BO and PM6:L8BO under AM1.5G irradiation (100 mW cm^{-2}).

BHJ film	V_{OC} (V)	J_{SC} (mA cm^{-2})	$J_{sc\ cal}$ (mA cm^{-2})	FF (%)	PCE (%)
Po2F/PM6:L8BO	0.880	26.95	25.38	80.34	19.05
PM6:L8BO	0.877	25.62	24.27	78.76	17.74

References

1 R. Po, G. Bianchi, C. Carbonera and A. Pellegrino, *Macromolecules*, 2015, **48**, 453-461.

2 D. Yuan, F. Pan, L. Zhang, H. Jiang, M. Chen, W. Tang, G. Qin, Y. Cao and J. Chen, *Solar RRL*, 2020, **4**, 2000062.

3 S. Wu, *J. Adhes.*, 1973, **5**, 39-55.

4 L. Bu, S. Gao, W. Wang, L. Zhou, S. Feng, X. Chen, D. Yu, S. Li and G. Lu, *Adv. Electron. Mater.*, 2016, **2**, 1600359.

5 Z. Wang, Y. Hu, T. Xiao, Y. Zhu, X. Chen, L. Bu, Y. Zhang, Z. Wei, B. B. Xu and G. Lu, *Adv. Opt. Mater.*, 2019, **7**, 1900152.

6 T. Xiao, J. Wang, S. Yang, Y. Zhu, D. Li, Z. Wang, S. Feng, L. Bu, X. Zhan and G. Lu, *J. Mater. Chem. A*, 2020, **8**, 401-411.

7 F.-Z. Cui, Z.-H. Chen, J.-W. Qiao, T. Wang, G.-H. Lu, H. Yin and X.-T. Hao, *Adv. Funct. Mater.*, 2022, **32**, 2200478.

8 X. e. Jia, Z. Chen, C. Duan, Z. Wang, Q. Yin, F. Huang and Y. Cao, *J. Mater. Chem. C*, 2019, **7**, 314-323.

9 S. Holliday, R. S. Ashraf, A. Wadsworth, D. Baran, S. A. Yousaf, C. B. Nielsen, C.-H. Tan, S. D. Dimitrov, Z. Shang, N. Gasparini, M. Alamoudi, F. Laquai, C. J. Brabec, A. Salleo, J. R. Durrant and I. McCulloch, *Nat. Commun.*, 2016, **7**, 11585.

10 H. Yao, D. Qian, H. Zhang, Y. Qin, B. Xu, Y. Cui, R. Yu, F. Gao and J. Hou, *Chin. J. Chem .* 2018, **36**, 491-494.

11 Y. Qin, M. A. Uddin, Y. Chen, B. Jang, K. Zhao, Z. Zheng, R. Yu, T. J. Shin, H. Y. Woo and J. Hou, *Adv. Mater.*, 2016, **28**, 9416-9422.

12 J. Xiao, X. e. Jia, C. Duan, F. Huang, H.-L. Yip and Y. Cao, *Adv. Mater.*, 2021, **33**, 2008158.

13 Q. Wang, M. Li, X. Zhang, Y. Qin, J. Wang, J. Zhang, J. Hou, R. A. J. Janssen and Y. Geng, *Macromolecules*, 2019, **52**, 4464-4474.

14 X. Yuan, Y. Zhao, Y. Zhang, D. Xie, W. Deng, J. Li, H. Wu, C. Duan, F. Huang and Y. Cao, *Adv. Funct. Mater.*, 2022, **32**, 2201142.

15 C. Yang, S. Zhang, J. Ren, M. Gao, P. Bi, L. Ye and J. Hou, *Energy Environ. Sci.*, 2020, **13**, 2864-2869.